THE JOURNAL OF PHYSICAL CHEMISTRY LETTERS
A JOURNAL OF THE AMERICAN CHEMICAL SOCIETY

pubs.acs.org/JPCL

Letter

Strong Isotopic Fractionation of Oxygen in TiO_2 Obtained by Surface-Enhanced Solid-State Diffusion

Heonjae Jeong and Edmund G. Seebauer*

Cite This: *J. Phys. Chem. Lett.* 2022, 13, 9841−9847

Read Online

ACCESS | Metrics & More | Article Recommendations | Supporting Information

ABSTRACT: Isotopically pure semiconductors have important applications for cooling electronic devices and quantum computing and sensing. Raw materials of sufficiently high isotopic purity are expensive and difficult to obtain; therefore, a post-synthesis method for removing isotopic impurities would be valuable. Through isotopic self-diffusion measurements of oxygen in rutile TiO_2 single crystals immersed in water, we demonstrate fractionation of ^{18}O by a factor of 3 below natural abundance in a near-surface region up to 10 nm wide. The submerged surface injects O interstitials that displace lattice ^{18}O deeper into the solid as a result of the statistics of interstitialcy-mediated diffusion combined with steep chemical gradients of O interstitials. Slightly acidic and slightly basic liquid solutions both enhance the fractionation and affect the details of isotopic profile shapes through several chemical and physical mechanisms.

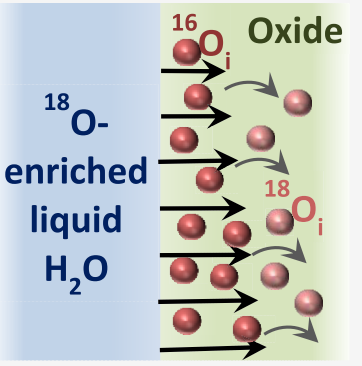

Use of isotopically pure semiconductors for enhancing electronic device performance has been investigated for several decades in connection with enhanced thermal conduction[1−5] and quantum computing and sensing.[6−8] Enhanced thermal conduction augments device cooling. In quantum devices, spinning nuclei require isolation from environmental perturbation by isotopically pure layers having nuclear spins of zero. Semiconductors having extraordinary isotopic purities required for these applications are insufficiently available, spurring the development of alternative purification techniques, e.g., in thin films that require little material.[6] One possible technique relies on isotopic fractionation by condensed phase diffusion. Mineralogists have long investigated this phenomenon,[9−13] which originates from small mass-dependent differences in atomic hopping frequencies. Fractionation is rather small: less than 1% for O,[14] a few percent for Ca, K, Ti, and Fe,[15] and up to tens of percent for low-mass elements, such as Li and Mg.[14,15] Large chemical concentration gradients boost fractionation,[10,14,15] and existing models imply that larger disparities in isotopic diffusivity would help even more.

One newly described[16,17] source of larger disparities arises as a statistical consequence of interstitialcy-mediated diffusion in solids. Steep gradients in the concentration of oxygen interstitials (O_i) may be produced by clean surfaces of several binary oxides, which inject sizable fluxes of O_i when contacted with liquid water near room temperature.[18] The equilibrium concentration of O_i at such temperatures is extremely small, so that sizable injected fluxes produce large concentration gradients. It is therefore plausible that substantial isotopic fractionation should occur near the surface. The present work demonstrates such fractionation for rutile TiO_2 single crystals. Variation of liquid pH alters the details of fractionation behavior by modulating the injection flux as well as other chemical and physical characteristics of the near-surface bulk. Isotopic self-diffusion experiments are used to monitor defect behavior, wherein cleaned and etched oxide specimens are submerged in water containing excess ^{18}O as a label. Oxygen enters the solid as O_i[18] and undergoes interstitialcy-mediated diffusion. Depth profiles of ^{18}O are measured afterward by secondary ion mass spectrometry (SIMS).

Figure 1 shows example ^{18}O concentration profiles after 1 h water exposures at pH values of 5 and 9, both at several temperatures. A striking feature, visible at both pH levels, is the large "valley" in label concentration near the surface that is up to about 10 nm wide. Counterintuitively, this isotopically depleted valley emerges, despite the enrichment of the liquid water to 10% ^{18}O. Depletion of the label within the valley region drives the ^{18}O concentration down to about a factor of 3 below the natural abundance level. ^{18}O lost from the valley builds up as a peak lying deeper in the bulk. The amount of ^{18}O contained within the peak exceeds the amount depleted from the valley, with the difference equaling the total amount of injected ^{18}O.

Figure 2 shows example ^{18}O concentration profiles after immersion in water at various temperatures for 1 h at pH 7. At

Received: August 10, 2022
Accepted: October 12, 2022

https://doi.org/10.1021/acs.jpclett.2c02490
J. Phys. Chem. Lett. 2022, 13, 9841−9847

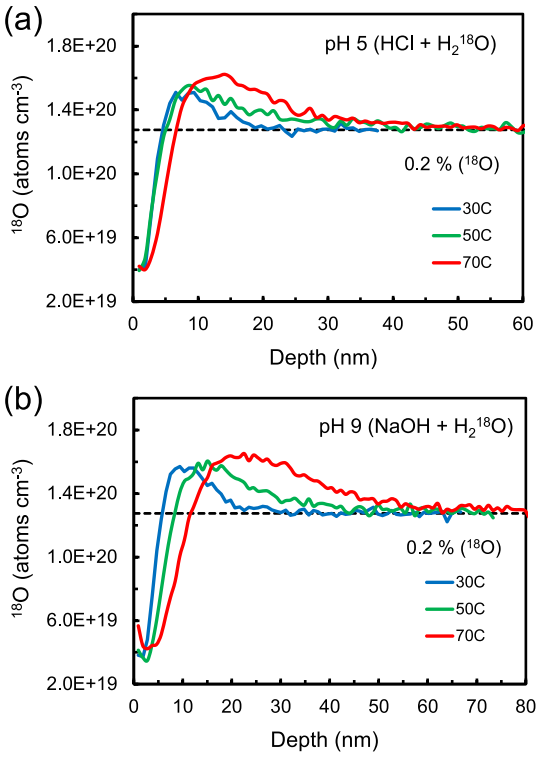

Figure 1. Example ^{18}O concentration profiles for $TiO_2(110)$ immersed in water at various temperatures for 1 h at pH levels of (a) 5 and (b) 9.

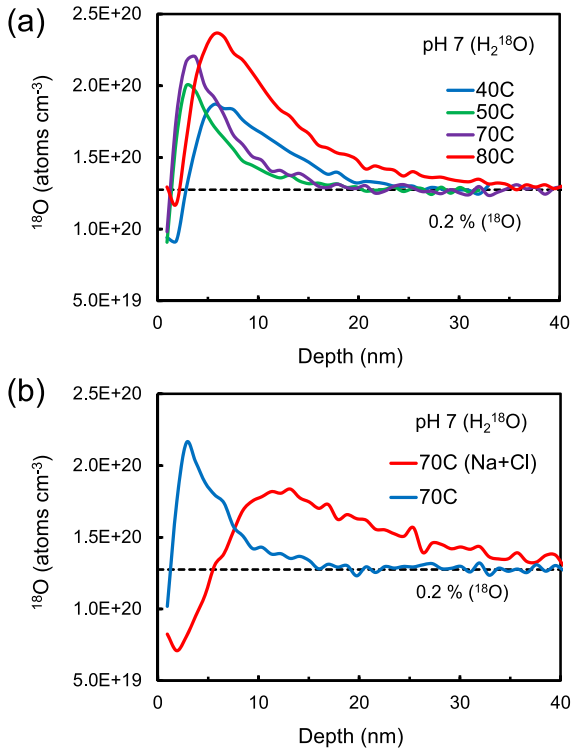

Figure 2. Example ^{18}O concentration profiles for $TiO_2(110)$ immersed in water for 1 h at pH 7 (a) at various temperatures and (b) at 70 °C with and without added NaCl. The salt-free profiles at 70 °C differ slightly in panels a and b because they represent measurements at two different locations on the same specimen.

pH 7, the valley is much narrower and less prominent than at pH 5 or 9. To quantify this effect, we define the valley width as the depth from the surface at which the ^{18}O concentration returns to the natural abundance level. The width increases with temperature from 3 to nearly 10 nm at pH 5 or 9 but actually decreases from 3 to 1 nm for pH 7. Adding both NaOH and HCl in concentrations equivalent to those at pH 5 or 9 (thereby making a salt solution of NaCl) strengthens fractionation to a magnitude lying between pH 7 and either 5 or 9.

Profile shapes sometimes exhibited noticeable variability in the near-surface region, especially at pH 7. X-ray photoelectron spectroscopy (XPS) combined with SIMS performed at several locations on single specimens as well as among specimens showed variable adsorption of adventitious impurities, especially carbon-containing species. Such species can act not only to poison injection sites but also to influence buildup of electrical charge on the surface. The resulting drift forces on charged interstitials can strongly affect the profile shape in the space charge layer near the surface.[19] Such adventitious adsorption proved difficult to control and often varied across the surface of a single specimen. It is also possible that variable concentrations of extended defects left over from initial mechanical polishing by the manufacturer contribute to profile variations by serving as traps for mobile O. Nevertheless, the primary trends described herein remained robust, even with such variations.

Some of the profiles in Figures 1 and 2 exhibit slight upturns in the ^{18}O concentration within the first nanometer of the surface. Profile shapes in this extremely shallow region suffer from distortions as a result of various well-known SIMS artifacts. However, the upturns occurred more prominently and commonly at pH 7 than for pH 5 or 9, which suggests that the upturn represents a qualitatively accurate description of the actual profiles.

Figure 3a shows Arrhenius plots of the valley width at all three values of pH. The effective activation energies of the changes with the temperature (Table S1 of the Supporting Information) are small, on the order of 0.1 eV or less. Figure 3b shows the net injection flux of F_{18} of ^{18}O in Arrhenius form for all three pH levels. Because the water is 10% isotopically pure in ^{18}O, the total flux F of O_i (all isotopes) may be computed as a factor of 10 greater than F_{18}, assuming (as in ref 18) that O_i injects with an isotopic makeup equal to that of the water. Although F_{18} at pH 5 and 9 (and with NaCl) is generally lower than that at pH 7, the activation energy of F_{18} is slightly higher (Table S1 of the Supporting Information).

We quantified the deeper portions of the profiles using two metrics: penetration depth and mean diffusion length (λ). Both parameters were computed as described in the Supporting Information, with corresponding results shown in Figure S1 of the Supporting Information. For pH 5, the penetration depth increases with the temperature from 10 to 50 nm, with λ increasing from 5 to 8 nm between 30 and 70 °C. For pH 9, the behavior is similar, with slightly larger values of 10−70 nm for the penetration depth and 4−17 nm for λ. These metrics show intermediate behavior at pH 7, with a range of 15−60 nm for the penetration depth and 5−11 nm for λ. Table S1 of the Supporting Information compares the activation energies for these metrics, which are all modest (0.2 eV or less) but are consistently lowest at pH 7.

Figure 4 shows numerous examples of ^{18}O concentration profiles at pH 7, comparing specimens initially exposed to

https://doi.org/10.1021/acs.jpclett.2c02490
J. Phys. Chem. Lett. 2022, 13, 9841−9847

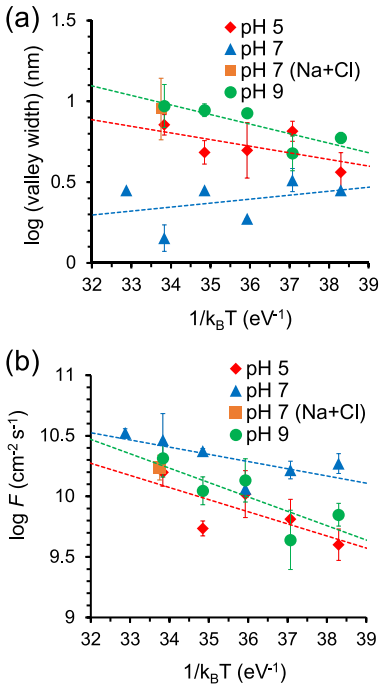

Figure 3. Arrhenius plots for (a) valley width and (b) net injection flux (F_{18}) for TiO_2(110) comparing conditions at pH levels of 5 and 9. Dashed lines represent linear least squares fits. Each point represents the average of profiles taken at three different locations on the surface of a specimen, typically for 2−4 distinct specimens. Confidence intervals were computed for all points; where no bars are visible, the range is narrower than the diameter of the data point.

room-temperature wet etching versus high-temperature annealing in O_2. Annealing eliminates some of the trapping sites for O_i that exist before self-diffusion starts. The near-surface isotopic fractionation is consistently larger for the room-temperature preparation, always reaching well below the natural abundance level, whereas the ^{18}O concentration rarely reaches appreciably below natural abundance with the annealing protocol.

The profile shapes described here resemble immensely amplified forms of the shapes typifying isotopic fractionation in mineral oxide melts containing Ge,[14] Ca,[14,15] and Li.[15] Related effects exist for solid-phase diffusion.[12,13] Although ^{18}O appears to diffuse against the gradient of the ^{18}O concentration in Figures 1 and 2, this phenomenon differs from "uphill diffusion" reported for dopants (without isotopic fractionation) in Si.[20−22] The peak in "uphill diffusion" resides at the surface (or an interface with SiO_2) and originates from interstitial trapping reactions there.

A mechanism involving interstitialcy-mediated diffusion can explain these effects based on hopping statistics combined with low label concentrations and steep interstitial gradients. An interstitialcy mechanism entails frequent exchange between atoms in the defect and on lattice sites. In general, the full ramifications of interstitialcy diffusion are understood less fully for semiconductors[23] and oxides[9] than for vacancy diffusion. In many oxides, including rutile TiO_2, O_i comprises two atoms arranged symmetrically about a regular O lattice site. For a dilute isotope, a labeled interstitial usually incorporates only one atom of the isotope. The two atoms within the defect hop with equal likelihood to recreate the interstitial at a neighboring lattice site. Therefore, a particular atom (^{18}O or

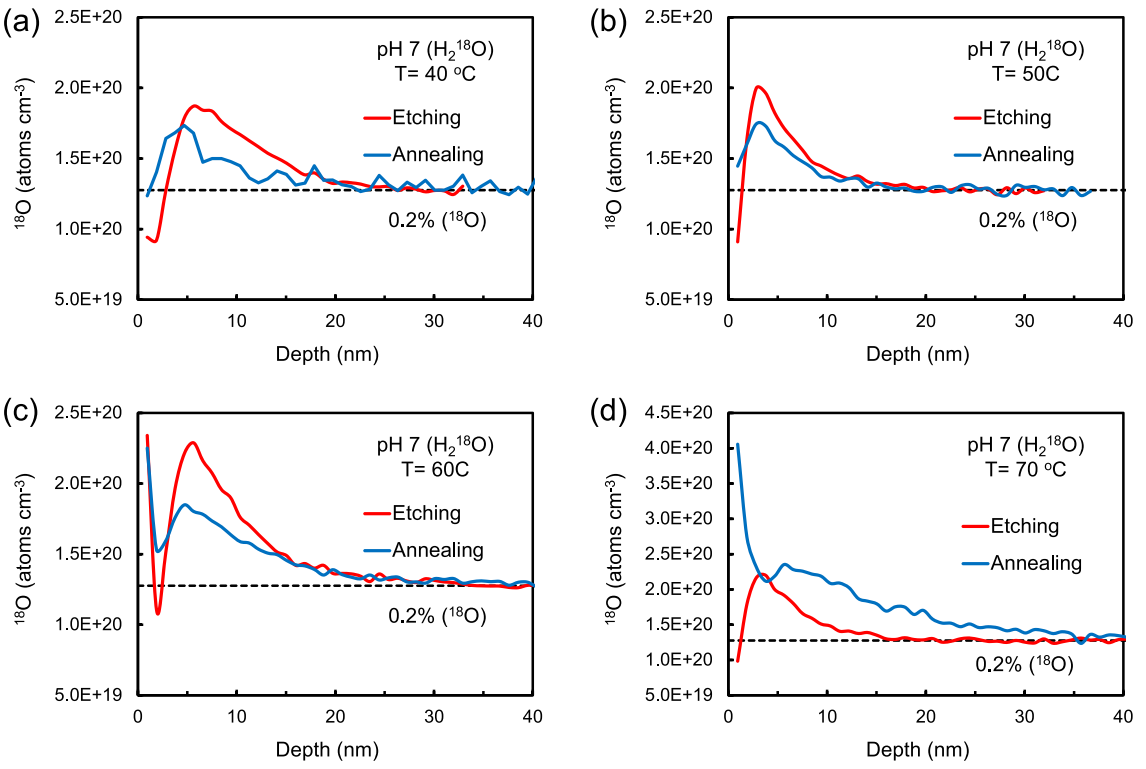

Figure 4. Example ^{18}O concentration profiles for 1 h at pH 7 at (a) 40 °C, (b) 50 °C, (c) 60 °C, and (d) 70 °C. Red and blue curves compare specimens exposed to room-temperature wet etching and high-temperature annealing in O_2. Annealing removes trapping sites for O_i and leads to gradients in the O_i concentration that are less sharp. The near-surface isotopic fractionation is correspondingly smaller, rarely reaching appreciably below the natural abundance level.

https://doi.org/10.1021/acs.jpclett.2c02490
J. Phys. Chem. Lett. 2022, 13, 9841−9847

^{16}O) within an interstitial typically executes only 2−3 hops before sequestering in the lattice.[16,17] Each hop conserves O_i as a chemical species, even though the constituent atoms vary. Immobilization of ^{18}O usually liberates a lattice ^{16}O. However, immobilization of ^{16}O usually liberates another ^{16}O, which allows ^{16}O to propagate for many atomic spacings before the release of ^{18}O breaks the chain. Only rarely can immobilization of ^{18}O release another ^{18}O in a similar fashion. Repeated over many hopping cycles, these statistics lower the mesoscale diffusivity of a particular isotope j by a factor of $[^jO_i]/[O_{i,total}]$, where $[O_{i,total}]$ represents the total O_i concentration summed over all isotopes. Here, "mesoscale" refers to a length scale longer than 2−3 hops but shorter than the mean diffusion length before trapping of O_i, which sets a ceiling on how far the chain-like propagation of an isotope can extend. For the present specimens "mesoscale" means roughly 2 to a few tens of nanometers. The natural abundance of ^{18}O is only 0.2% compared to 99.8% for ^{16}O. In the absence of interstitial trapping, the ratio of mesoscale diffusivities D^{16}/D^{18} is 500 at the natural abundance concentration and grows larger as ^{18}O becomes more dilute.

The steep gradients arise partly from the low bond coordination of O adsorbed on clean metal oxide surfaces, which facilitates creation of O_i[17,18] with barriers below roughly 1 eV.[18] These injection barriers, combined with even lower bulk hopping barriers, enable clean oxide surfaces exposed to liquid water to inject O_i at substantial rates, even near room temperature. Because the equilibrium concentration of O_i in this regime is vanishingly small, fast injection initially creates a sharp interstitial gradient. ^{18}O liberated as O_i from the lattice is pulled deeper into the bulk by this strong gradient. Moreover, the isotopic disparity in diffusivity enables $^{16}O_i$ to race far ahead of $^{18}O_i$, which biases the isotopic composition of interstitials at the leading edge of the interstitial diffusion front toward ^{16}O. These combined effects enable ^{16}O to replace much of ^{18}O present originally in the lattice, pushing displaced ^{18}O deeper into the bulk and creating a valley and peak isotopic profile shape. The net effect loosely resembles that of a snowplow acting on ^{18}O.

The slight upturn in the ^{18}O concentration next to the surface observed for some specimens presumably corresponds to the label originating from water (distinguished from those already present in the lattice) that has propagated far enough to become barely visible in SIMS.

The profiles in Figure 4 comparing wet etching and annealing protocols demonstrate the importance of steep gradients in the O_i concentration. In single-crystal TiO_2, whose surface has been cleaned by wet etching at room temperature, many traps for O_i remain in the bulk, including O vacancies (V_O) and extrinsic elements, such as H. V_O reacts with O_i by mutual annihilation, while interstitial H reacts to form O_i−H_i complexes.[18] In contrast, high-temperature annealing in O_2 (650−800 °C with oxygen partial pressures between 5×10^{-6} and 6×10^{-5} Torr) not only cleans the surface but also injects O_i.[17] This injection eliminates V_O down to a depth of several hundred nanometers and may also result in some volatilization of hydrogen. Thus, fewer traps exist to react with O_i during subsequent water exposure. The lessened trapping enables the concentration profile of O_i to smoothen more rapidly, thereby leading to O_i gradients that are less sharp. Accordingly, annealed crystals exhibit lessened isotopic fractionation, leading to less pronounced valleys in Figure 4.

This physical picture relies upon an interstitialcy mechanism, distinguished from an interstitial mechanism, wherein a single interstitial diffuses many lattice spacings before becoming trapped or kicking into the lattice. The latter mechanism would not produce the large isotopic disparity in diffusivity that strong fractionation requires. A more refined description of interstitialcy-mediated fractionation would allow for slight isotopic differences in hopping rates as a result of different vibrational frequencies and zero point energies. However, these effects represent only minor perturbations on the primary governing factors: hopping statistics and sharp gradients.

Solution acidity or basicity affects the details of the profile shapes through several mechanisms. Four distinct pH-dependent effects may be at play simultaneously, including changes in the O_i trapping efficiency within the bulk, in the net injection flux, in the value of the Fermi energy (E_F) at the surface as a result of adsorption, and in the value of E_F at the surface as a result of the inability of the bulk to compensate for excess charge at the interface. Sophisticated process simulators akin to those available for ion implantation in microelectronic devices[24,25] would be required to model these effects quantitatively, but the following paragraphs describe the qualitative basis for each of them.

Spatial and temporal changes in the O_i trapping efficiency of the bulk arise for two reasons. First, O_i eliminates donor V_O over time in a progressively wider region near the surface. Second, O_i forms complexes with a variety of intrinsic and extrinsic defects. Many such complexes exist in multiple charge states whose concentrations (i.e., ability to trap and hold O_i) depend upon the local value of E_F.[18] The concentrations of these complexes become spatially dependent if excess charge on the surface creates a space charge layer (SCL), so that E_F varies with depth. Solution pH exerts its effects through acid−base reactions between the surface and water that typically lead to a net charge on the TiO_2 surface. Dependent upon the degree of buildup and the ionization levels of the relevant trapping complexes, spatial variations will arise in their concentrations. As O_i penetrates progressively deeper into the solid, temporal variations will also arise.

In the particular case of rutile TiO_2, excess negative charge probably resides at the surface over most or all of the pH range examined here, giving rise to a depletion-type SCL in n-type rutile containing a positive space charge. The reason is that the isoelectric point for rutile [equivalent to the point of zero charge (PZC) if no specific adsorption occurs[26]] varies with incorporated impurities[27] and roughness[28] but averages about pH 5,[29−32] with a standard deviation of about 0.8.[32] O_i acts as an acceptor, and the complexes that it forms tend to be less donor-like (or more acceptor-like) than the corresponding uncomplexed defect traps. This effect, combined with the progressive elimination of donor V_O mentioned above, should decrease the overall concentration of donors in the SCL and contribute to its progressive widening.

A second mechanism by which pH affects the profile shape is through the net injection flux. F represents the mathematical difference between the rates of injection and annihilation and depends upon pH through three distinct mechanisms. The first two mechanisms involve the rates of elementary-step injection and re-incorporation through the concentration of injectable O and the rate constants for surface injection and annihilation. The coverage of OH (i.e., the singly deprotonated precursor to injectable O) varies with pH,[33,34] with complete deprotonation occurring only for pH > 13.[34] Also, the activation energies[17]

https://doi.org/10.1021/acs.jpclett.2c02490
J. Phys. Chem. Lett. 2022, 13, 9841−9847

and probably the pre-exponential factors for both injection and re-incorporation depend upon E_F at the surface as a result of changes in the charge state of the chemical intermediates involved in injection. E_F at the surface depends upon the pH of the liquid through the amount of negatively charged OH that is adsorbed. The third mechanism involves the drift component to the motion of O_i in the SCL. O_i exists in the −2 charge state in bulk rutile for E_F greater than about 0.9 eV.[35] With the pH-dependent buildup of negative charge on the surface as described above, the electric field in the SCL repels negatively charged mobile defects, such as O_i, from the surface,[36] thereby impeding re-incorporation.

A third mechanism by which pH affects the profile shape involves temporal changes in E_F at the surface as a result of slow adsorption of adventitious impurities, including various carbon-containing species. These species not only poison injection sites but may also enhance or inhibit acid−base reactions between the surface and water that lead to surface charge buildup. Such adventitious adsorption is difficult to control and can vary across the surface of a single specimen. Such effects probably contribute to the confidence intervals shown in Figure 3.

A fourth mechanism by which pH affects the profile shape involves changes in surface E_F resulting from the ability of the bulk to compensate for excess charge at the surface. For thin films and nanostructures possessing a limited bulk volume, the ability of the bulk to compensate for excess charge at the interface is compromised.[38] Indeed, E_F at the surface may vary with time as a result of progressive neutralization of donor traps by O_i, as described above. In the absence of applied bias potential, it unfortunately remains an unsolved problem in surface science to compute self-consistently the net charge accumulation resulting from acid−base interactions in the presence of partial compensation by both ion adsorption from the electrolyte and SCL formation in the solid. A relationship between pH and PZC for d^0 oxides, such as TiO_2, has been proposed only in the past decade,[37] and a relationship between E_F and pH under conditions far from the PZC remains unknown. Moreover, ions of opposite charge from the electrolyte may partly compensate for charge buildup from acid−base reactions, as suggested by the NaCl data of Figure 2.

The data presented here demonstrate isotopic purification of O by about a factor of 3 from natural abundance levels in a region up to 10 nm wide. Mesoscale simulation models are necessary to predict ultimate limitations on the width of the isotopically purified region, the degree of purification possible during a single exposure, and the dependence of these parameters on conditions, such as the injected flux, isotopic purity of the water, temperature, electrolyte concentration, and other factors. However, several qualitative notions are already clear.

First, the concept of isotopic purification by interstitialcy diffusion is not specific to oxygen. If another chemical element diffuses by an interstitialcy mechanism, the physical picture also applies as long as a sharp gradient in the interstitial concentration can be generated in a solid having large disparities in the isotopic concentration. For example, Ti diffuses by an interstitialcy mechanism along the [110] direction.[39] Methods for efficient generation of interstitials at surfaces remain in their infancy but already exist for both O[16−18] using both gas and liquid-based methods and Ti[40] using gas methods. For the highest isotopic purity with little buildup of unwanted isotopes near the surface, it is advisible to use a source of interstitials that are enriched in the desired isotope.

Second, repeated cycles of interstitial injection should lead to improved isotopic purity. As the interstitials penetrate the bulk diffusively over time, their gradients become less sharp. Smaller interstitial gradients enable random diffusion to smooth out and perhaps eliminate the valley. Pausing the injection at intervals enables the injected interstitials to disperse and sequester in trap sites at the modest temperatures used here, where equilibrium interstitial concentrations are low. Successive cycles of injection generate fresh waves of interstitials that re-establish sharp gradients.

Third, interstitial injection works best as a strategy for post-synthesis isotopic purification of layers that already possess substantial enrichment. The disparity among isotopic diffusivities grows as the solid becomes more isotopically pure. Initial material synthesis (e.g., by chemical vapor deposition) may not require special precautions for the constituent element, such as O, whose natural abundance is already strongly dominated by a single isotope. For applications in quantum spin isolation, for example, the lone stable isotope of oxygen having a non-zero spin is ^{17}O, whose natural abundance is only 0.04%. For an element like Ti, however, the zero-spin majority isotope (^{48}Ti) has a natural abundance of only 74%. The stable isotopes with non-zero spin are ^{47}Ti (7.4%) and ^{49}Ti, respectively, present at 7.4 and 5.4%. Thus, initial material synthesis with isotopically enriched ^{48}Ti would be advisible.

In conclusion, through isotopic self-diffusion measurements of oxygen in rutile TiO_2 single crystals immersed in water, we demonstrate fractionation of ^{18}O by a factor of 3 below natural abundance in a near-surface region up to 10 nm wide. Isotopic purification of ^{16}O near the surface is governed by the statistics of interstitialcy-mediated diffusion combined with steep chemical gradients of O interstitials originating from the submerged surface. Slightly acidic and slightly basic liquid solutions both enhance the fractionation, which represents an example of using liquid-surface chemistry (via pH) to control the defect-surface chemistry. There is no reason to believe this fundamental physical picture is restricted only to oxygen or TiO_2. As an approach to post-synthesis isotopic purification, higher purities are likely to be reached through repeated pause and inject cycles. Interstitialcy diffusion is common among elements in both single-component and compound semiconductors, suggesting that this approach to isotopic purification may find extensive use as methods for interstitial injection from surfaces continue to develop.

■ ASSOCIATED CONTENT

Supporting Information

The Supporting Information is available free of charge at https://pubs.acs.org/doi/10.1021/acs.jpclett.2c02490.

Materials and methods, including specification of TiO_2 specimens, sample preparation using wet etching, isotopic self-diffusion experiments, XPS measurement conditions, SIMS measurement conditions, and analytical fitting method, supporting figures, including Arrhenius plots for penetration depth and λ for TiO_2 and post-diffusion surface composition measured by XPS, and supporting table for activation energies for F, valley width, penetration depth, and λ (PDF)

https://doi.org/10.1021/acs.jpclett.2c02490
J. Phys. Chem. Lett. 2022, 13, 9841−9847

AUTHOR INFORMATION

Corresponding Author

Edmund G. Seebauer − *Department of Chemical and Biomolecular Engineering, University of Illinois at Urbana−Champaign, Urbana, Illinois 61801, United States;* orcid.org/0000-0002-4722-3901; Email: eseebaue@illinois.edu

Author

Heonjae Jeong − *Department of Mechanical Science and Engineering, University of Illinois at Urbana−Champaign, Urbana, Illinois 61801, United States;* orcid.org/0000-0003-4452-049X

Complete contact information is available at: https://pubs.acs.org/10.1021/acs.jpclett.2c02490

Notes

The authors declare no competing financial interest.

ACKNOWLEDGMENTS

This work was supported by the U.S. National Science Foundation under Grant DMR 17-09327. SIMS and XPS measurements were performed in the Materials Research Laboratory Central Research Facilities, University of Illinois at Urbana−Champaign.

REFERENCES

(1) Inyushkin, A. V.; Taldenkov, A. N.; Yakubovsky, A. Y.; Markov, A. V.; Moreno-Garsia, L.; Sharonov, B. N. Thermal Conductivity of Isotopically Enriched ^{71}GaAs Crystal. *Semicond. Sci. Technol.* **2003**, *18* (7), 685−688.

(2) Inyushkin, A. V.; Taldenkov, A. N.; Ager, J. W.; Haller, E. E.; Riemann, H.; Abrosimov, N. V.; Pohl, H.-J.; Becker, P. Ultrahigh Thermal Conductivity of Isotopically Enriched Silicon. *J. Appl. Phys.* **2018**, *123* (9), 095112.

(3) Lindsay, L.; Broido, D. A.; Reinecke, T. L. Thermal Conductivity and Large Isotope Effect in GaN from First Principles. *Phys. Rev. Lett.* **2012**, *109* (9), 95901.

(4) Li, X.; Zhang, J.; Puretzky, A. A.; Yoshimura, A.; Sang, X.; Cui, Q.; Li, Y.; Liang, L.; Ghosh, A. W.; Zhao, H.; Unocic, R. R.; Meunier, V.; Rouleau, C. M.; Sumpter, B. G.; Geohegan, D. B.; Xiao, K. Isotope-Engineering the Thermal Conductivity of Two-Dimensional MoS_2. *ACS Nano* **2019**, *13* (2), 2481−2489.

(5) Haller, E. E. Isotopically Engineered Semiconductors. *J. Appl. Phys.* **1995**, *77* (7), 2857−2878.

(6) England, J.; Cox, D.; Cassidy, N.; Mirkhaydarov, B.; Perez-Fadon, A. Investigating the Formation of Isotopically Pure Layers for Quantum Computers Using Ion Implantation and Layer Exchange. *Nucl. Instrum Methods Phys. Res. B* **2019**, *461*, 30−36.

(7) Itoh, K. M.; Watanabe, H. Isotope Engineering of Silicon and Diamond for Quantum Computing and Sensing Applications. *MRS Commun.* **2014**, *4* (4), 143−157.

(8) Kane, B. E. A Silicon-Based Nuclear Spin Quantum Computer. *Nature* **1998**, *393* (6681), 133−137.

(9) van Orman, J. A.; Krawczynski, M. J. Theoretical Constraints on the Isotope Effect for Diffusion in Minerals. *Geochim. Cosmochim. Acta* **2015**, *164*, 365−381.

(10) Teng, F.-Z.; McDonough, W. F.; Rudnick, R. L.; Walker, R. J. Diffusion-Driven Extreme Lithium Isotopic Fractionation in Country Rocks of the Tin Mountain Pegmatite. *Earth Planet Sci. Lett.* **2006**, *243* (3), 701−710.

(11) Dauphas, N.; Teng, F.-Z.; Arndt, N. T. Magnesium and Iron Isotopes in 2.7 Ga Alexo Komatiites: Mantle Signatures, No Evidence for Soret Diffusion, and Identification of Diffusive Transport in Zoned Olivine. *Geochim. Cosmochim. Acta* **2010**, *74* (11), 3274−3291.

(12) Watson, E. B.; Müller, T. Non-Equilibrium Isotopic and Elemental Fractionation during Diffusion-Controlled Crystal Growth under Static and Dynamic Conditions. *Chem. Geol.* **2009**, *267* (3), 111−124.

(13) Dauphas, N. Diffusion-Driven Kinetic Isotope Effect of Fe and Ni during Formation of the Widmanstätten Pattern. *Meteorit Planet Sci.* **2007**, *42* (9), 1597−1613.

(14) Richter, F. M.; Liang, Y.; Davis, A. M. Isotope Fractionation by Diffusion in Molten Oxides. *Geochim. Cosmochim. Acta* **1999**, *63* (18), 2853−2861.

(15) Richter, F. M.; Davis, A. M.; DePaolo, D. J.; Watson, E. B. Isotope Fractionation by Chemical Diffusion between Molten Basalt and Rhyolite. *Geochim. Cosmochim. Acta* **2003**, *67* (20), 3905−3923.

(16) Jeong, H.; Li, M.; Kuang, J.; Ertekin, E.; Seebauer, E. G. Mechanism of Creation and Destruction of Oxygen Interstitial Atoms by Nonpolar Zinc Oxide(10−10) Surfaces. *Phys. Chem. Chem. Phys.* **2021**, *23*, 16423−16435.

(17) Jeong, H.; Ertekin, E.; Seebauer, E. G. Kinetic Control of Oxygen Interstitial Interaction with TiO_2(110) via the Surface Fermi Energy. *Langmuir* **2020**, *36* (42), 12632−12648.

(18) Jeong, H.; Ertekin, E.; Seebauer, E. G. Surface-Based Post-Synthesis Manipulation of Point Defects in Metal Oxides Using Liquid Water. *ACS Appl. Mater. Interfaces* **2022**, *14* (29), 34059−34068.

(19) Gorai, P.; Seebauer, E. G. Kinetic Model for Electric-Field Induced Point Defect Redistribution near Semiconductor Surfaces. *Appl. Phys. Lett.* **2014**, *105* (2), 021604.

(20) Duffy, R.; Venezia, V. C.; Loo, J.; Hopstaken, M. J. P.; Verheijen, M. A.; Van Berkum, J. G. M.; Maas, G. C. J.; Tamminga, Y.; Dao, T.; Demeurisse, C. Low-Temperature Diffusion of High-Concentration Phosphorus in Silicon, a Preferential Movement toward the Surface. *Appl. Phys. Lett.* **2005**, *86* (8), 081917.

(21) Ferri, M.; Solmi, S.; Parisini, A.; Bersani, M.; Giubertoni, D.; Barozzi, M. Arsenic Uphill Diffusion during Shallow Junction Formation. *J. Appl. Phys.* **2006**, *99* (11), 113508.

(22) Ferri, M.; Solmi, S.; Giubertoni, D.; Bersani, M.; Hamilton, J. J.; Kah, M.; Kirkby, K.; Collart, E. J. H.; Cowern, N. E. B. Uphill Diffusion of Ultralow-Energy Boron Implants in Preamorphized Silicon and Silicon-on-Insulator. *J. Appl. Phys.* **2007**, *102* (10), 103707.

(23) Fahey, P. M.; Griffin, P. B.; Plummer, J. D. Point Defects and Dopant Diffusion in Silicon. *Rev. Mod. Phys.* **1989**, *61* (2), 289−384.

(24) Moroz, V.; Oh, Y.-S.; Pramanik, D.; Graoui, H.; Foad, M. A. Optimizing Boron Junctions through Point Defect and Stress Engineering Using Carbon and Germanium Co-Implants. *Appl. Phys. Lett.* **2005**, *87* (5), 051908.

(25) Sibaja-Hernandez, A.; Wei Xu, M.; Decoutere, S.; Maes, H. TSUPREM-4 Based Modeling of Boron and Carbon Diffusion in SiGeC Base Layers under Rapid Thermal Annealing Conditions. *Mater. Sci. Semicond. Process* **2005**, *8* (1), 115−120.

(26) Kosmulski, M. The pH Dependent Surface Charging and Points of Zero Charge. VIII. Update. *Adv. Colloid Interface Sci.* **2020**, *275*, 102064.

(27) Kosmulski, M. The pH-Dependent Surface Charging and the Points of Zero Charge. *J. Colloid Interface Sci.* **2002**, *253* (1), 77−87.

(28) Borghi, F.; Vyas, V.; Podestà, A.; Milani, P. Nanoscale Roughness and Morphology Affect the IsoElectric Point of Titania Surfaces. *PLoS One* **2013**, *8* (7), No. e68655.

(29) Dobson, K. D.; Connor, P. A.; McQuillan, A. J. Monitoring Hydrous Metal Oxide Surface Charge and Adsorption by STIRS. *Langmuir* **1997**, *13* (10), 2614−2616.

(30) Connor, P. A.; Dobson, K. D.; McQuillan, A. J. Infrared Spectroscopy of the TiO_2/Aqueous Solution Interface. *Langmuir* **1999**, *15* (7), 2402−2408.

(31) Bullard, J. W.; Cima, M. J. Orientation Dependence of the Isoelectric Point of TiO_2 (Rutile) Surfaces. *Langmuir* **2006**, *22* (24), 10264−10271.

(32) Kosmulski, M. The Significance of the Difference in the Point of Zero Charge between Rutile and Anatase. *Adv. Colloid Interface Sci.* **2002**, *99* (3), 255−264.
(33) Crawford, S.; Thimsen, E.; Biswas, P. Impact of Different Electrolytes on Photocatalytic Water Splitting. *J. Electrochem. Soc.* **2009**, *156* (5), H346.
(34) Imanishi, A.; Okamura, T.; Ohashi, N.; Nakamura, R.; Nakato, Y. Mechanism of Water Photooxidation Reaction at Atomically Flat TiO_2 (Rutile) (110) and (100) Surfaces: Dependence on Solution pH. *J. Am. Chem. Soc.* **2007**, *129* (37), 11569−11578.
(35) Jeong, H.; Seebauer, E. G.; Ertekin, E. First-Principles Description of Oxygen Self-Diffusion in Rutile TiO_2: Assessment of Uncertainties Due to Enthalpy and Entropy Contributions. *Phys. Chem. Chem. Phys.* **2018**, *20* (25), 17448−17457.
(36) Dev, K.; Jung, M. Y. L.; Gunawan, R.; Braatz, R. D.; Seebauer, E. G. Mechanism for Coupling between Properties of Interfaces and Bulk Semiconductors. *Phys. Rev. B* **2003**, *68* (19), 195311.
(37) Nandakumar, N. K.; Seebauer, E. G. Relating Catalytic Activity of d0 Semiconducting Metal Oxides to the Fermi Level Position. *J. Phys. Chem. C* **2014**, *118* (13), 6873−6881.
(38) Nandakumar, N. K.; Seebauer, E. G. Manipulating Reaction Rates of Metal-Oxide Heterogeneous Catalysts via Semiconductor Heterojunctions. *J. Phys. Chem. C* **2018**, *122* (29), 16655−16663.
(39) Iddir, H.; Öğüt, S.; Zapol, P.; Browning, N. D. Diffusion Mechanisms of Native Point Defects in Rutile TiO_2: Ab Initio Total-Energy Calculations. *Phys. Rev. B* **2007**, *75* (7), 73203.
(40) Gilliard, K. L.; Seebauer, E. G. Manipulation of Native Point Defect Behavior in Rutile TiO_2 via Surfaces and Extended Defects. *J. Phys.: Condens. Matter* **2017**, *29* (44), 445002.

https://doi.org/10.1021/acs.jpclett.2c02490
J. Phys. Chem. Lett. 2022, 13, 9841−9847